Electron Spin Echo Envelope Modulation Study of Oxygenated Iron−Cobalt Hybrid Hemoglobins Reveals Molecular Features Analogous to Those of the Oxy Ferrous Protein†

H. Caroline Lee*,‡ and Jack Peisach‡,§

Departments of Molecular Pharmacology and of Physiology and Biophysics, Albert Einstein College of Medicine of Yeshiva University, Bronx, New York 10461

Antonio Tsuneshige and Takashi Yonetani

Department of Biochemistry and Biophysics, University of Pennsylvania School of Medicine, Philadelphia, Pennsylvania 19104

Received December 8, 1994; Revised Manuscript Received March 16, 1995⊗

ABSTRACT: Two oxygenated iron−cobalt hybrid hemoglobins (Hbs), $(\alpha Co-O_2\beta Fe-O_2)_2$ and $(\alpha Fe-O_2\beta Co-O_2)_2$, were studied by electron spin echo envelope modulation (ESEEM) spectroscopy in order to measure (i) electron-nuclear hyperfine and nuclear quadrupole coupling to the N_ϵ of the proximal histidyl imidazole and (ii) nuclear hyperfine coupling to exchangeable ^2H in the oxyCo subunits. ^{14}N couplings were found to be smaller in the oxyCo α subunits than in the oxyCo β subunits, suggesting a more ionic and shorter $Co-O_2$ bond in the α subunits [Lee et al. (1994) *Biochemistry 33*, 7609], which correlates with the higher O_2 affinity found for $(\alpha Co\beta Fe-O_2)_2$ Hb than for $(\alpha Fe-O_2\beta Co)_2$ Hb [Imai et al. (1980) *J. Mol. Biol. 138*, 635]. A smaller nuclear quadrupole coupling constant found for the proximal histidyl N_ϵ in the oxyCo α subunits also suggests an increase in the overlap between the N_ϵ sp^2 hybrid and the Co d_{z^2} orbital, i.e., a shorter $Co-N_\epsilon$ bond, than in the oxyCo β subunits. On the other hand, the relative orientation of the **g** and $^{14}N_\epsilon$ nuclear quadrupole tensors, obtained by spectral simulation, suggests that the Co−O−O bond angle is similar in the two types of oxyCo subunits. An X-ray crystallographic study of oxyFe Hb A [Shaanan, B. (1982) *Nature 296*, 683] has also reported similar Fe−O−O bond angles in both α and β subunits, but with shorter $Fe-N_\epsilon$ and $Fe-O_2$ bonds in the α subunits. A hyperfine-coupled ^2H was detected in the spectra of D_2O-exchanged samples of both hybrid Hbs, although the resolution was only marginal in $(\alpha Fe-O_2\beta Co-O_2)_2$ Hb. These results support the idea of the presence of a hydrogen bond to bound O_2 in both oxyCo α and β subunits.

Our recent applications of ESEEM[1] spectroscopy (Mims & Peisach, 1989) to oxyCo-substituted globins, functional and paramagnetic analogues of Fe(II) O_2-carrying hemoproteins (Hoffman & Petering, 1970), demonstrate the feasibility of correlating electronic structure with molecular structure and O_2 affinity (Lee et al., 1992, 1993, 1994a). ESEEM spectra of oxyCo globins arise from coupling of the unpaired electron on bound O_2 (Hoffman et al., 1970; Getz et al., 1975; Dedieu et al., 1976; Tovrog et al., 1976) to the Co-bound N_ϵ of the proximal histidyl imidazole (Magliozzo et al., 1987; Lee et al., 1992). The ESEEM-revealed $^{14}N_\epsilon$ nuclear hyperfine and quadrupole couplings are modulated by the electronic configuration of the *trans* $Co-O_2$ bond. These couplings decrease with an increase in the ionicity of the $Co-O_2$ bond (Lee et al., 1994a); i.e., the electronic configuration more likely resembles $Co^{3+}-O_2^{\bullet-}$ rather than $Co^{2+}-O_2$. With greater ionicity of the $Co-O_2$ bond, O_2 affinity is expected to increase due to an increase in the O_2 character of the σ-bonding orbital, $sp^2(N) + d_{z^2}(Co) + \pi^*(O_2)$ (Lee et al., 1992). Indeed, Co globins that exhibit higher O_2 affinity have consistently shown a reduction in electron-nuclear couplings (Lee et al., 1992, 1993, 1994a).

Besides functional properties, electron-nuclear couplings can also be correlated with molecular structure. The size of the Co−O−O bond angle, for example, can be obtained from the determination of the relative orientation of the *z* axis of the **g** with the $^{14}N_\epsilon$ nuclear hyperfine and the nuclear quadrupole tensors by simulation of spectra (Lee et al., 1994a) (see Discussion). Furthermore, the $^{14}N_\epsilon$ nuclear quadrupole coupling constant can also be used to assess the $Co-N_\epsilon$ bond length. This parameter is related to the magnitude of the electric field gradient along the $Co-N_\epsilon$ bond (Hsieh et al., 1977; Ashby et al., 1978) and decreases with an increase in the overlap between the N_ϵ lone-pair-containing sp^2 hybrid and the Co d_{z^2} orbital, i.e., with a shortening of the $Co-N_\epsilon$ bond.

To further understand the correlation between the electronic structure, molecular structure, and functional properties of oxyCo globins, we have conducted an ESEEM study of the oxyCo subunits of two fully oxygenated Fe−Co hybrid Hbs: $(\alpha Co-O_2\beta Fe-O_2)_2$ and $(\alpha Fe-O_2\beta Co-O_2)_2$ (Tsuneshige

† This work was supported by NIH Grants GM40168 (J.P.), RR02538 (J.P.), and HL14508 (T.Y.).

* Author to whom correspondence should be addressed.

‡ Department of Molecular Pharmacology, Albert Einstein College of Medicine of Yeshiva University.

§ Department of Physiology and Biophysics, Albert Einstein College of Medicine of Yeshiva University.

⊗ Abstract published in *Advance ACS Abstracts,* May 1, 1995.

[1] Abbreviations: CW, continuous wave; EPR, electron paramagnetic resonance; ESEEM, electron spin echo envelope modulation; Hb, hemoglobin A; sw Mb, sperm whale myoglobin; NQI, nuclear quadrupole interaction; RR, resonance Raman.

0006-2960/95/0434-6883$09.00/0

& Yonetani, 1994, and references therein). Here, only the oxyCo subunits are ESEEM-active, and structural information obtained by ESEEM spectroscopy is used to compare the α and β subunits in an oxygenated tetramer and to correlate the differences in electronic structure with known differences in their functional properties (Imai et al., 1980; Ikeda-Saito & Yonetani, 1980). Furthermore, we compare subunit differences in molecular features such as metal−axial ligand bond length and metal−O−O bond angle for the oxyCo subunits with the corresponding oxyFe subunits in oxyFe Hb (Shaanan, 1982, 1983).

This ESEEM study also aims at understanding the nature of the interaction between the bound O_2 and the nearby distal histidine in the two types of oxyCo subunits. A resonance Raman study (Kitagawa et al., 1982) of the same oxy Fe−Co hybrid Hbs examined in this ESEEM investigation has suggested the presence of a hydrogen bond between the distal histidine and bound O_2 in *both* types of oxyCo subunits, based on D_2O effect on ^{18}O-sensitive bands. These results are inconsistent with those of an X-ray crystallographic study of oxyFe Hb (Shaanan, 1982, 1983), which suggests that the distal hydrogen bond is present in the oxyFe α subunits but absent in the β subunits. However, the conclusion of the RR study of Kitagawa et al. (1982) needs to be reevaluated because the original assignment of ^{18}O-sensitive bands as pure O−O stretching modes in oxyCo globins has subsequently been questioned (Bruha & Kincaid, 1988; Proniewicz & Kinkaid, 1990) so that the observed D_2O effects on these RR bands cannot be used as direct evidence for the presence of a hydrogen bond to bound O_2.

The issue of hydrogen bonding in the two types of oxyCo subunits is addressed here by an ESEEM study of D_2O-exchanged samples. The assignment of a hydrogen bond between bound O_2 and a nearby exchangeable ^2H is based on ^2H hyperfine coupling arguments (Lee et al., 1992, 1993, 1994a). The present ESEEM study detects hyperfine-coupled ^2H for both types of oxyCo subunits of oxy Co−Fe hybrid Hbs, although the resolution for the oxyCo β subunits is only marginal (see Results). These results suggest the presence of a hydrogen bond to the bound O_2 in both oxyCo α and β subunits, supporting the conclusion drawn by Kitagawa et al. (1982).

MATERIALS AND METHODS

Protein Preparation. Fe−Co hybrid Hbs were prepared according to published procedures (Yonetani et al., 1974a; Ikeda−Saito et al., 1977).

Samples for EPR and ESEEM measurements were exchanged, by ultrafiltration, with 0.1 M Hepes buffer, pH 7, in H_2O or D_2O (90 atom %) and were frozen in liquid nitrogen in air. CW EPR measurements indicated that all the Co subunits were fully oxygenated (Yonetani et al., 1974b). Since the O_2 affinity of the Fe subunits is 50 times higher than the Co subunits (Yonetani et al., 1974), it can be concluded that the tetramers were fully oxygenated. Final protein concentrations were 1.2−1.6 mM or 0.6−0.8 mM in Co. pH meter reading of the D_2O buffer was not corrected for isotope effects.

Spectroscopy. CW EPR spectra were obtained at 77 K on a Varian E112 spectrometer equipped with a Systron-Donner frequency counter.

ESEEM data were recorded at liquid helium temperatures (1.4−4.2 K) on a pulsed EPR spectrometer described previously (McCracken et al., 1987), using both transmission cavities (Mims, 1974) and folded stripline cavities (Britt & Klein, 1987) that can accommodate 4 mm, o.d., EPR tubes. Three pulse, or simulated echo, experiments (Peisach et al., 1979) were conducted at microwave frequencies between 8.5 and 10.7 GHz. The time interval between the first and the second microwave pulses, τ, was chosen as a multiple of the ^1H Larmor frequency in order to suppress modulations from weakly coupled ^1H (Peisach et al., 1979). Data were collected at the time $2\tau + T$, where T is the time interval between the second and third pulses. Each data set contained 1024 points; each point represented the average of 50−200 measurements of the integrated electron spin echo. The spectra presented are cosine Fourier transformations of the time domain data subsequent to dead time reconstruction (Mims, 1984). Spectra are normally collected at at least three magnetic field settings (g = 2.08, 2.03, 1.99) and three τ values for each setting.

Computer Simulation. CW EPR spectra were simulated using a modified version of the program QPOWA (Belford & Nilges, 1979; Nilges, 1981; Maurice, 1981) using line widths of 25, 15, and 15 MHz in the x, y, z directions, respectively. Spectra of D_2O-exchanged samples were used as references for the simulations because of the improved resolution of ^{59}Co hyperfine lines in this solvent.

The computer program for simulation of ESEEM spectra has been described previously (Cornelius et al., 1990). The input parameters for a simulation are (i) the principal values of the **g** and ^{59}Co ($I = {}^7/_2$) nuclear hyperfine tensors, obtained from simulation of frozen solution CW EPR spectra, (ii) experimental parameters that include microwave frequency, magnetic field strength, and the τ value, and (iii) parameters for the ^{14}N spin Hamiltonian:

$$\hat{\mathbf{H}}_N = -g_N\beta_N\mathbf{BI} + \mathbf{SA}_N\mathbf{I} + (e^2qQ/4) \times [3I_z^2 + 2 + \eta(I_x^2 - I_y^2)] \quad (1)$$

where **B** is the magnetic field, **S** and **I** are respectively the electron spin and the nuclear spin operators, and β is the Bohr magnetron. The first, second, and third terms of eq 1 represent respectively the nuclear Zeeman, nuclear hyperfine, and nuclear quadrupole interactions. The nuclear hyperfine tensor, $\mathbf{A}_N$, is taken to be axial, with principal values $A_{iso} - F$, $A_{iso} - F$, and $A_{iso} + 2F$ (Cornelius et al., 1990). A_{iso} is the isotropic nuclear hyperfine coupling constant, $F = g_N\beta_N g_e\beta_e/(r_{eff})^3$ is the anisotropic coupling constant, and r_{eff} is the effective dipole distance. Two angles, θ_N and ϕ_N, relate the orientation of the nuclear hyperfine and **g** tensors. The NQI is described by a nuclear quadrupole coupling constant, e^2qQ, and an asymmetry factor, η, which are related to the principal values (q_{xx}, q_{yy}, q_{zz}) of the electric field gradient tensor by

$$e^2qQ = e^2q_{zz}Q \quad (2)$$

$$\eta = (q_{yy} - q_{xx})/q_{zz} \quad (3)$$

where $|q_{zz}| > |q_{yy}| > |q_{xx}|$. Three Euler angles, α, β, and γ, relate the orientations of the NQI and the **g** tensors.

All simulations were performed on a Microvax II computer.

RESULTS

ESEEM of Oxy Fe−Co Hybrid Hbs. ESEEM spectra of the two oxy Fe−Co hybrid Hbs (Figure 1) arise from

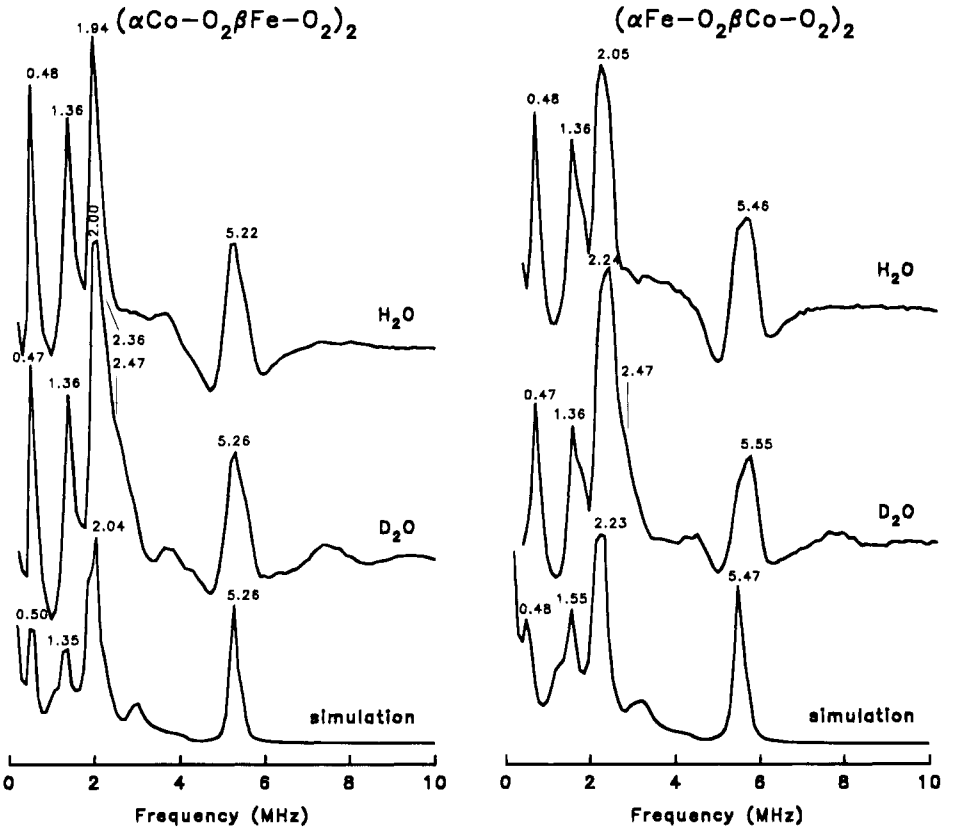

FIGURE 1: (Left panel) ESEEM spectrum of (αCo−O_2βFe−O_2)$_2$ Hb (top) in 0.1 M Hepes, pH 6.78, and H_2O, collected at 9.9626 GHz, 3506 G (g = 2.03), τ = 201 ns, and temperature = 4.2 K, and (middle) in 0.1 M Hepes, pH 7.06, and D_2O, collected at 9.9145 GHz, 3490 G (g = 2.03), τ = 202 ns, and temperature = 4.2 K. Simulation (bottom) of the H_2O spectrum using parameters given in Table 1 and g and ^{59}Co hyperfine values obtained from simulation of the CW EPR spectrum (Figure 2). (Right panel) ESEEM spectrum of (αFe−O_2βCo−O_2)$_2$ Hb (top) in 0.1 M Hepes, pH 6.78, and H_2O, collected at 9.9624 GHz, 3506 G (g = 2.03), τ = 201 ns, and temperature = 4.2 K, and (middle) in 0.1 M Hepes, pH 7.06, and D_2O, collected at 9.9217 GHz, 3492 G (g = 2.03), τ = 202 ns, and temperature = 4.2 K. Simulation (bottom) of the H_2O spectrum using parameters given in Table 1 and g and ^{59}Co hyperfine values obtained from simulation of the CW EPR spectrum (Figure 2).

electron-nuclear coupling to the N_ϵ of the proximal histidyl imidazole in the oxyCo subunits (Magliozzo et al., 1987; Lee et al., 1992). These spectra are typical for an $S = {}^1/_2$ center weakly coupled to a ligand ^{14}N under conditions of near exact cancellation (Flanagan & Singel, 1987), where the magnitude of the nuclear Zeeman interaction of the coupled ^{14}N nucleus is close to half of that of the nuclear hyperfine interaction (Mims & Peisach, 1978). The spectra normally consist of three sharp, low-frequency lines and a broad, high-frequency line. The low-frequency lines arise from the electron spin manifold where the nuclear Zeeman term and the nuclear hyperfine term in the ^{14}N spin Hamiltonian (eq 1) cancel each other. At exact cancellation, these are the "zero-field" quadrupole resonance lines (ν_0, ν_-, ν_+), and their frequencies are related to the nuclear quadrupole coupling constant, e^2qQ, and the asymmetry factor, η, by

$$\nu_\pm = {}^3/_4 e^2qQ(1 \pm \eta/3) \quad (4)$$

$$\nu_0 = {}^1/_2 e^2qQ\cdot\eta \quad (5)$$

The broad, high-frequency line arises from the other electron spin manifold where the nuclear hyperfine interaction adds to the nuclear Zeeman interaction, resulting in a $\Delta m_I = 2$ transition (Mims & Peisach, 1978). For the oxyCo subunits of both hybrid Hbs, the $\Delta m_I = 2$ line occurs at 5.2−5.6 MHz (Figure 1) at a microwave frequency near 10 GHz.

The ESEEM spectra of the two hybrid Hbs are analyzed by computer simulation using g and Co hyperfine values obtained from simulation of the CW EPR spectra (Figure 2) and following a procedure described previously (Lee et al., 1994a). Thus in a typical simulation, the coupling parameters A_{iso}, e^2qQ, η, and r_{eff} (see Materials and Methods) are first varied to obtain a frequency match for data collected at g = 2.03. The angles $\beta(=\theta_N)$ (Lee et al., 1994a) (also see Discussion) and α are then varied simultaneously in increments of 10° from 0° to 90° [i.e., for each value for the angle $\beta(=\theta_N)$, ten values for the angle α are used, and vice versa] to obtain the best intensity and line-shape match for the g = 2.03 spectrum. Often more than one set of angles (β, θ_N, α) are obtained from simulations of the g = 2.03 spectrum. Spectra collected at two other g values (1.99, 2.08) are then simulated (with adjustment of the coupling parameters obtained for the g = 2.03 setting) to determine a set of angles (β, θ_N, α) based on the following criteria. The angles should (i) best produce the general shape (i.e., the number of lines and their relative intensity) of the low-frequency region of ESEEM spectra obtained at different g values, a region most sensitive to variations of the angles α and β, (ii) match the shape of the high-frequency $\Delta m_I = 2$ line, which is most sensitive to variations of θ_N, and (iii) require the least adjustment of the coupling parameters to fit data at different g values. The range of parameters used in fitting spectra collected at the three g values (using a single set of angles)

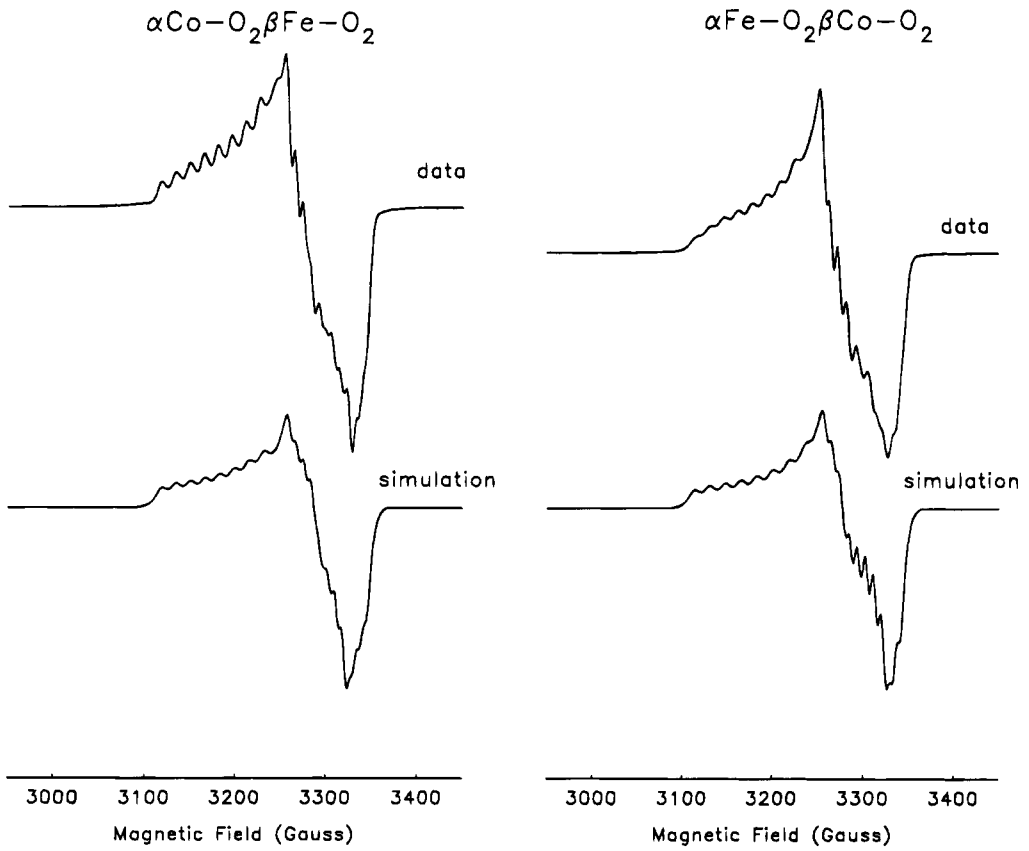

FIGURE 2: (Left panel) (top) CW EPR spectrum of $(\alpha Co-O_2\beta Fe-O_2)_2$ Hb in 0.1 M Hepes, pH 7.06, and D_2O, measured at 9.2307 GHz, modulation amplitude = 5 G, modulation frequency = 100 kHz, and temperature = 77 K, and (bottom) simulation using $g_x = 2.0775$, $g_y = 2.0045$, $g_z = 1.9870$, $A_{xx}^{Co} = 47$ MHz, $A_{yy}^{Co} = 24$ MHz, and $A_{zz}^{Co} = 21$ MHz. (Right panel) (top) CW EPR spectrum of $(\alpha Fe-O_2\beta Co-O_2)_2$ Hb in 0.1 M Hepes, pH 7.06, and D_2O, measured at 9.2303 GHz, modulation amplitude = 5 G, modulation frequency = 100 kHz, and temperature = 77 K, and (bottom) simulation using $g_x = 2.0776$, $g_y = 2.0041$, $g_z = 1.9915$, $A_{xx}^{Co} = 51$ MHz, $A_{yy}^{Co} = 26$ MHz, and $A_{zz}^{Co} = 24$ MHz.

Table 1: Electron-Nuclear Coupling Parameters for the Proximal Histidyl N_ϵ of Co-Substituted Subunits in Oxy Fe−Co Hybrid Hemoglobins[a]

hybrid Hb	A_{iso} (MHz)	r_{eff} (Å)	θ (deg)	ϕ^b (deg)	e^2qQ (MHz)	η	α (deg)	β (deg)	γ^c (deg)
$(\alpha Co-O_2\beta Fe-O_2)_2$[d]	2.90	3.60	40	0	2.03	0.48	20	40	0
$(\alpha Fe-O_2\beta Co-O_2)_2$[e]	3.07	3.60	40	0	2.32	0.36	20	40	0

[a] The width of the microwave pulses used in these experiments normally leads to transitions within ±20 G of the magnetic field setting. Incorporation of this pulse width into the simulations was found to have no effect on the intensities or frequencies of the spectra components. Therefore, all simulations were carried out using a single input resonance magnetic field in order to expedite the simulations. [b] Since the ^{14}N hyperfine tensor is assumed to be axial (see above), A_{xx}^N and A_{yy}^N can be along any direction in the xy plane, so the angle ϕ_N is assumed to be 0°. Variation of this angle has almost no effect on the simulations. [c] Variation of γ by 10° changes the relative intensities of the spectral components slightly but does not improve the fits, so this angle is taken to be 0° in the simulations. [d] The range of values for A_{iso} is 0.11 MHz, for e^2qQ is 0.19 MHz, and for η is 0.13. [e] The range of values for A_{iso} is 0.02 MHz, for e^2qQ is 0.08 MHz, and for η is 0.09.

defines the uncertainties in the simulations. The effects of varying ϕ_N and γ (from 0° to 90°) on the simulations are then evaluated independently using the previously determined values for β, θ_N, and α (see footnotes *a*−*c* of Table 1).

In simulations of ESEEM spectra of oxyCo globins (Lee et al., 1992, 1993, 1994a), including those of the two oxy Fe−Co hybrid Hbs in this study (Figure 1), the best-fit spectra do not always produce an exact match of the relative intensity of all four $^{14}N_\epsilon$ spectral components at every experimental g or τ value. A possible explanation is that the low-frequency region contains contribution from the porphyrin nitrogens (Magliozzo et al., 1987). Nevertheless, the simulations are sensitive to a change of ≥10° for the angles β (=θ_N) and α such that a set of angles can be chosen on the basis of the procedure and criteria described above.

The nuclear hyperfine and nuclear quadrupole coupling parameters for the coupled proximal histidyl N_ϵ in the oxyCo subunits of both hybrid Hbs are summarized in Table 1. Both the $^{14}N_\epsilon$ nuclear hyperfine and nuclear quadrupole coupling constants are larger for oxyCo β subunits than for the oxyCo α subunits. On the other hand, similar values for the angles θ_N, β, and α are found for both types of oxyCo subunits.

ESEEM of Oxy Fe−Co Hybrid Hbs in D_2O. A comparison of the ESEEM spectra of D_2O-exchanged oxy Fe−Co hybrid Hbs and those of the H_2O samples is given in Figure 1. These spectra are collected at a τ value (see Materials and Methods) equals to 3 times the proton periodicity at the applied magnetic field of ≈3500 G. The resolution of ^2H ESEEM components is compromised at lower τ values and magnetic field because, under such experimental conditions, the electron spin echo envelope is dominated by modulations due to coupled ^{14}N. At 9.9 GHz, 3490 G (g = 2.03), two components at 2.36 and 2.47 MHz, not observed in the corresponding H_2O spectrum (Figure 1, top left spectrum),

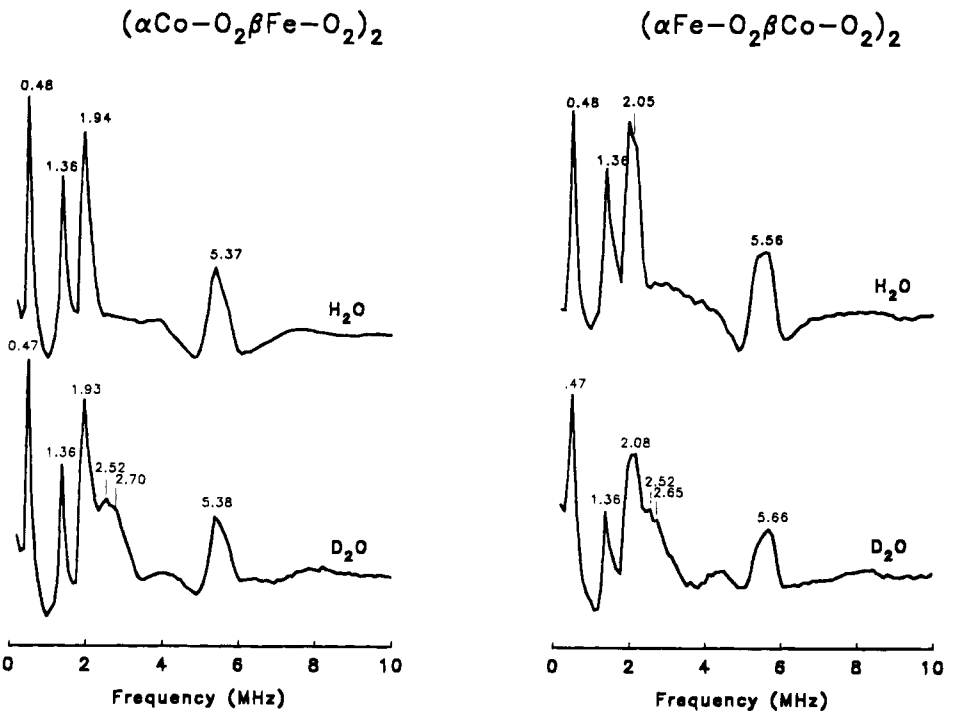

FIGURE 3: (Left panel) ESEEM spectrum of (αCo−O_2βFe−O_2)$_2$ Hb (top) in 0.1 M Hepes, pH 6.78, and H_2O, collected at 10.5996 GHz, 3731 G (g = 2.03), τ = 189 ns, and temperature = 4.2 K, and (bottom) in 0.1 M Hepes, pH 7.06, and D_2O, measured at 10.727 GHz, 3776 G (g = 2.03), τ = 187 ns, and temperature = 4.2 K. (Right panel) ESEEM spectrum of (αFe−O_2βCo−O_2)$_2$ Hb (top) in 0.1 M Hepes, pH 6.78, and H_2O, collected at 10.4068 GHz, 3681 G (g = 2.03), τ = 191 ns, and temperature = 4.2 K and (bottom) at 10.678 GHz, 3758 G (g = 2.03), τ = 187 ns, and temperature = 4.2 K.

were resolved for D_2O-exchanged (αCo−O_2βFe−O_2)$_2$ Hb (Figure 1, middle left spectrum). At 10.7 GHz, 3776 G (g = 2.03) (Figure 3, bottom left spectrum), the features not observable in the corresponding H_2O spectrum (Figure 3, top left spectrum) are found at 2.52 and 2.70 MHz. The shifts (+0.16, +0.23 MHz) are similar to the increase in ^{2}H Zeeman energy (+0.17 MHz). These features are therefore attributed to coupled exchangeable ^{2}H. Similarly for (αFe−O_2βCo−O_2)$_2$ Hb, the D_2O spectrum collected at 9.9 GHz, 3490 G (g = 2.03) (Figure 1, middle right spectrum), contains a 2.24-MHz peak and a marginally resolved shoulder at 2.47 MHz that are not found in the corresponding H_2O spectrum (Figure 1, top right spectrum). These components shift +0.28 and +0.18 MHz with an increase in ^{2}H Zeeman energy of +0.17 MHz (Figure 3, bottom right spectrum) and can thus be attributed to coupled ^{2}H as well.

The ^{2}H components in the D_2O spectra of the two hybrid Hbs are assigned as follows. The 2.36 and 2.24 MHz lines in the 9.9 GHz spectra (^{2}H Larmor frequency = 2.28 MHz) (Figure 1) and the 2.52 MHz line in the 10.7 GHz spectra (^{2}H Larmor frequency = 2.47 MHz) (Figure 3) above appear at frequencies near the ^{2}H Larmor frequency and arise from dipole-coupled ^{2}H, for example, those from solvent. ^{2}H features that are offset from the Larmor frequency arise from ^{2}H that are hyperfine-coupled to the electron spin. The frequencies of these components are described by

$$\nu(^2\mathrm{H}) = \nu(^2\mathrm{H})^{\mathrm{Larmor}} \pm {}^1/_2|A_{\mathrm{eff}}| \qquad (6)$$

where A_{eff} is the effective hyperfine coupling constant since the nuclear quadrupole coupling of ^{2}H in these systems is assumed to be negligible (Mims & Peisach, 1989). Therefore, for both oxy Fe−Co hybrid Hbs, A_{eff} is close to 0.4 MHz. However, it must be pointed out that, due to the poor resolution of the shoulder at 2.47 MHz in the 9.9 GHz spectrum of (αFe−O_2βCo−O_2)$_2$ Hb (Figure 1, middle right spectrum), it is not possible to determine definitively that the 2.65 MHz component in the corresponding 10.7 GHz spectrum (Figure 3, bottom right spectrum) arises from ^{2}H by means of its dependency on the ^{2}H Zeeman energy. Therefore, while ESEEM demonstrates the presence of hyperfine-coupled ^{2}H in the oxyCo α subunits of (αCo−O_2βFe−O_2)$_2$ Hb, the assignment of ^{2}H in the oxyCo β subunits of (αFe−O_2βCo−O_2)$_2$ Hb is less firm. Also, the resolution of ^{2}H components does not allow us to determine whether the magnitude of the hyperfine coupling is different in the two types of oxyCo subunits.

DISCUSSION

Electron-Nuclear Coupling to the Proximal Histidyl N_ϵ. Smaller nuclear hyperfine and nuclear quadrupole couplings to the proximal histidyl N_ϵ are found for the oxyCo α subunits than for the oxyCo β subunits of oxy Co−Fe hybrid Hbs (Table 1). As $^{14}N_\epsilon$ nuclear hyperfine coupling in oxyCo globins occurs through induced spin polarization of the fully occupied σ orbital [$sp^2(N_\epsilon)$ + d_{z^2}(Co) + π*(O_2)] (Wayland & Abd-Elmageed, 1974) and decreases with an increase in the O_2 character in this orbital, reduced $^{14}N_\epsilon$ nuclear hyperfine coupling signifies an increase in the ionicity of the Co−O_2 bond, or a shift toward the $Co^{3+}-O_2^{\bullet -}$ configuration. Previous ESEEM studies of oxyCo globins have consistently found that the ionicity of the Co−O_2 bond (electron-nuclear coupling for the proximal histidyl N_ϵ) is well correlated with O_2 affinity (Lee et al., 1992, 1993, 1994a). As for the two oxy Fe−Co hybrid Hbs, higher O_2 affinity[2] has been reported for the oxyCo α subunits (Imai et al., 1980), in which the present ESEEM study demonstrates a more ionic Co−O_2 bond. This increase in the ionicity of the Co−O_2 bond may

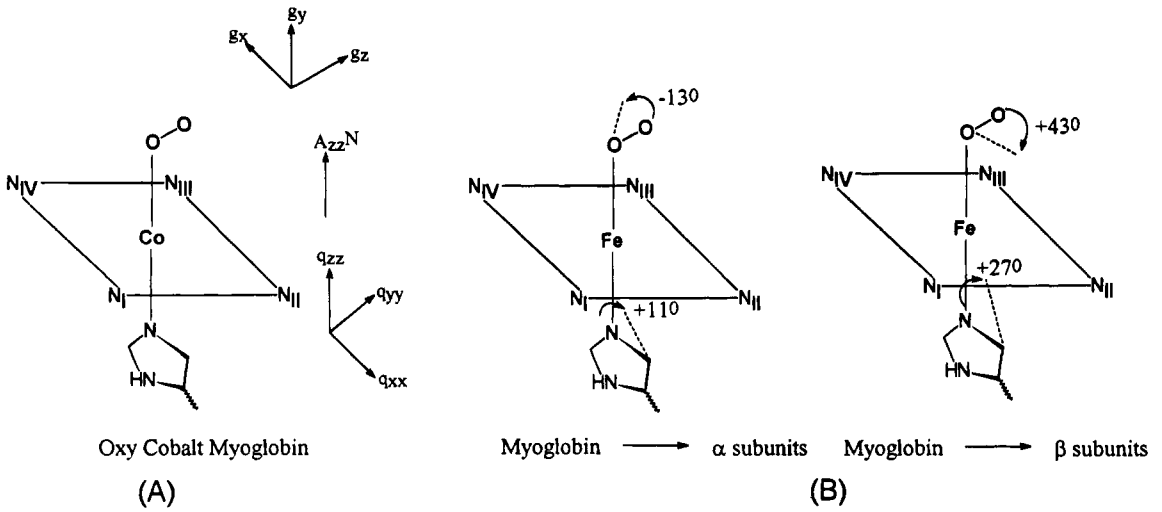

FIGURE 4: (A) Schematic representation of the magnetic tensor orientation of oxyCo globins, based on a single crystal EPR (Hori et al., 1982) and an X-ray crystallographic (Petsko et al., 1978) study of oxyCo Mb. (B) Comparison of the molecular structure of the heme site of oxyferrous Mb and Hb, based on X-ray crystal structures (Phillips, 1980; Shaanan, 1983). Dotted lines represent the positions of the O−O bond and the proximal imidazole $C_\delta-C_\epsilon$ axis in the oxyFe Hb subunits. The numbering of the pyrrole nitrogens follows the convention of Fermi (1975).

also explain the faster O_2 dissociation rate for the oxyCo β subunits in $(\alpha Fe-CO\beta Co-O_2)_2$ Hb than for the oxyCo α subunits in $(\alpha Co-O_2\beta Fe-CO)_2$ Hb (Ikeda-Saito & Yonetani, 1980). [These Fe−CO/Co−O_2 hybrid Hbs show ESEEM spectra identical to those of their corresponding fully oxy counterparts (data not shown)]. Thus the previously proposed relationship between electronic structure and O_2 affinity for oxyCo globins is again confirmed by our findings for the two oxy Fe−Co hybrid Hbs.

The differences in electronic structure found for the two types of oxyCo subunits can also be used to correlate differences in molecular structure. The smaller nuclear quadrupole coupling constant for the oxyCo α subunit as compared to the oxyCo β subunits indicates a decrease in the electric field gradient along the proximal histidyl N_ϵ lone-pair-containing sp^2 hybrid as a result of increased lone-pair donation to Co (Hsieh et al., 1977; Ashby et al., 1978). This suggests an increase in the overlap between the N_ϵ sp^2 hybrid and the Co d_{z^2} orbital, i.e., a shortening of the Co−N_ϵ bond in the oxyCo α subunits. This finding parallels an X-ray crystal structure of oxyFe Hb (Shanaan, 1982, 1983), where the Fe−N_ϵ bond in the α subunits is shorter than its counterparts in the β subunits by 0.11 Å. Furthermore, the increase in ionicity of the Co−O_2 bond in the oxyCo α subunits, as compared to the oxyCo β subunits of the hybrid Hbs, based on smaller $^{14}N_\epsilon$ couplings, implies a shorter Co−O_2 bond for the oxyCo α subunits than for the oxyCo β subunits. An analogous structure is found for oxyFe Hb where the Fe−O_2 bond is 1.67 Å in the α subunits as compared to 1.83 Å in the β subunits (Shaanan, 1982, 1983).

Geometry of the Two Axial Co−Ligand Bonds. Molecular features other than the Co−N_ϵ and the Co−O_2 bond lengths can be obtained from the relative orientation of the **g**, $^{14}N_\epsilon$ nuclear hyperfine, and nuclear quadrupole tensors of the oxyCo subunits, based on computer simulation of ESEEM spectra. This is achieved by using the room temperature **g** tensor assignment of oxyCo sw Mb, obtained from an X-ray crystal structure (Petsko et al., 1978) and a single crystal EPR study (Hori et al., 1980, 1982), as reference (Lee et al., 1994a) (Figure 4A). Thus for the oxyCo subunits of the two hybrid Hbs, the **g** tensor is determined by the O−O bond direction, with g_z (g_{min}) along the O−O axis and g_x (g_{max}) along the unpaired electron-containing π^* orbital of bound O_2 (Hori et al., 1980, 1982). A_{zz}^N and q_{zz} are assumed to be coincident (Magliozzo et al., 1987) and to lie along the Co−N_ϵ bond (Wayland & Abd-Elmageed, 1974; Hsieh et al., 1977; Ashby et al., 1978). For this reason, the angle β is assumed to be equal to θ_N in spectral simulations.[3] The angle between g_z and q_{zz} (A_{zz}^N), β ($=\theta_N$), gives an estimate of the Co−O−O bond angle. q_{yy} is taken to be along the p_π orbital of the proximal histidyl N_ϵ (Hsieh et al., 1977; Ashby et al., 1978). The angle between this axis and g_x provides the relative orientation of the O−O bond and the proximal imidazole plane.

A similar value for angle β ($=\theta_N = 40°$) (Table 1) is used to generate best-fit ESEEM spectra for the two oxy Fe−Co hybrid Hbs, suggesting that the Co−O−O bond angle, ≈140°, is similar for both types of oxyCo subunits. This value is larger than the Co−O−O bond angle, 125°, found for oxyCo sw Mb at room temperature (Petsko et al., 1978; Hori et al., 1980).[4] A structural analogy is observed for oxyFe Hb, where the Fe−O−O bond angles of the two types of oxyFe subunits (Shaanan, 1982, 1983) are 153° and 159° and are larger than the Fe−O−O angle of 115° found in

[2] The comparison of O_2 affinity of the two oxy Fe−Co Hbs is based on the equilibrium constants (K_{assoc}) for these two processes: $(\alpha Co)_2(\beta Fe-O_2)_2 + O_2 \rightarrow (\alpha Co-O_2)(\alpha Co)(\beta Fe-O_2)_2$, $K_{assoc} = 0.057$ $(mmHg)^{-1}$, and $(\alpha Fe-O_2)_2(\beta Co)_2 + O_2 \rightarrow (\alpha Fe-O_2)_2(\beta Co-O_2)(\beta Co)$, $K_{assoc} = 0.031$ $(mmHg)^{-1}$ (Imai et al., 1980). Note that the $K_{assoc} = 0.057$ $(mmHg)^{-1}$ was erroneously published in Imai et al. (1980) as 0.0057 $(mmHg)^{-1}$ in the bottom right scheme of Figure 4.

[3] In previous simulations of ESEEM spectra of oxyCo globins, it was observed that using an input θ_N of $\leq \beta - 20°$ did not produce a match in the line shape of the $\Delta m_I = 2$ line (Lee et al., 1994a), supporting the assumption that q_{zz} and A_{zz}^N are nearly coincident.

[4] The Co−O−O bond geometry was found to change when crystals of oxyCo Mb were frozen (Hori et al., 1980, 1982). Two species of equal absorption were observed in the CW EPR spectrum. Both contain a larger Co−O−O bond angle than that found in room temperature. One species (species I) has its O−O bond axis directed toward pyrrole II; the other (species II) has its O−O bond axis directed toward pyrrole III.

oxyFe sw Mb (Phillips, 1980). The crystal structure of oxyFe Hb (Shanaan, 1982, 1983) shows an upward movement (from heme) of the terminal oxygen (and the distal residues), as compared to oxyFe sw Mb (Phillips, 1980). Shanaan (1983) suggests that the larger distal heme pocket in oxyFe Hb as compared to oxyFe sw Mb (Phillips, 1980) accounts for the larger Fe−O−O bond angle found for the oxyFe Hb subunits. One might infer from the larger Co−O−O bond angles found for the oxyCo subunits of oxy Fe−Co hybrid Hbs, as compared to oxyCo sw Mb, that the differences in distal heme pocket structures found between oxyFe Hb and oxyFe sw Mb are retained in the oxy Co−Fe hybrid Hbs and oxyCo Mb; i.e., the distal heme pocket of the two oxy Co−Fe hybrid Hbs is larger than that in oxyCo Mb. On the other hand, an ESEEM study of oxyCo human Mb distal histidine (E7) mutants (Lee et al., 1994a) has found that the Co−O−O bond angle does not correlate with the size of the E7 side chain and therefore possibly not with the size of the distal heme pocket.

Computer simulation also finds an angle α of 20° for the oxyCo α and oxyCo β subunits of the hybrid Hbs (Table 1). This angle α, between q_{yy} and g_y, is related to the relative orientation of the O−O axis and the proximal imidazole plane (Figure 4A). For example, in oxyCo sw Mb (Petsko et al., 1978; Hori et al., 1980) [and oxyFe sw Mb as well (Phillips, 1980)] at room temperature,[4] the proximal imidazole plane is parallel to the pyrrole N_{II}−pyrrole N_{IV} axis, and the projection of the O−O axis is directed toward pyrrole III, such that the p_π orbital of the proximal histidyl N_ϵ (q_{yy}) is perpendicular to the unpaired electron-containing π^* orbital of bound O_2 (g_x) or parallel to g_y. Thus the angle $\alpha \approx 0°$.

Figure 4B compares the relative orientation of the O−O bond and the proximal imidazole in oxyFe sw Mb with those in the two types of subunits of oxyFe Hb, $(\alpha Fe-O_2\beta Fe-O_2)_2$, on the basis of the crystal structures of the two proteins (Phillips, 1980; Shanaan, 1982, 1983). The O−O bond in the α subunits of oxyFe Hb is rotated 13° counterclockwise from that in oxyFe sw Mb, while the proximal imidazole plane is rotated 11° clockwise from that in oxyFe sw Mb. In the β subunits of oxyFe Hb, the O−O bond is rotated 43° clockwise from that in oxyFe sw Mb while the proximal imidazole plane is rotated 27° clockwise from that in Mb. If the orientation of the O−O bond and the proximal imidazole plane in the oxyCo α subunits of $(\alpha Co-O_2\beta Fe-O_2)_2$ Hb differs from those in oxyCo sw Mb in a similar fashion as in the two oxyFe proteins, the p_π orbital of the proximal histidyl N_ϵ of the oxyCo α subunits of the hybrid will make an angle of 114° with the unpaired electron-containing π^* orbital of O_2, and α is predicted to be 24°. Similarly, assuming that the two axial ligands in oxyCo β subunits of $(\alpha Fe-O_2\beta Co-O_2)_2$ Hb retain the orientation found in the β in oxyFe Hb (Figure 4B), the p_π orbital of the proximal histidyl N_ϵ makes an angle of 74° with the O_2 unpaired electron-containing π^* orbital, and the angle α is predicted to be 16°.

An angle α of 20° is found for the oxyCo α and oxyCo β subunits of the two hybrid Hbs. This value for the angle α is similar to that predicted from the crystal structures of oxyFe sw Mb and oxyFe Hb. However, an angle α of 20° merely suggests that the O−O bond axis makes an angle of ≈70° with the proximal imidazole plane. It does not provide any information on the orientation of the two axial ligands in the protein, for example, with respect to the porphyrin nitrogens. In order to compare the orientation of the O−O bond in the oxyCo subunits of the two hybrid Hbs with the oxyFe counterparts in oxyFe Hb, the proximal imidazole in the oxyCo subunits of the hybrid Hbs is assumed to retain the orientation found in a crystal structure of oxyFe Hb (Shaanan, 1982, 1983). This assumption is reasonable since the orientation of the proximal imidazole in oxyCo sw Mb (Petsko et al., 1978) is the same as that in the oxyFe protein (Phillips, 1980). Similarly, the orientation of the proximal histidine in deoxyCo human Hb (Fermi et al., 1982) is the same as that in the deoxyFe protein (Fermi et al., 1984). Provided that the orientation of the proximal imidazole of the oxyCo subunits of the hybrid Hbs is that found in the respective oxyFe counterparts, the agreement between the values for the angle α obtained from computer simulation of ESEEM spectra and those predicted from crystal structures of the oxyFe proteins as described above suggests that the O−O bond in the oxyCo subunits of the hybrids can only orient in one of the following ways: (i) similar to that of the respective oxyFe counterparts or (ii) 180° away from the orientation found in the crystal structure of the oxyFe Hb. We rule out the second possibility because of the detection of hyperfine-coupled exchangeable ^2H that are most likely on the distal histidine (see below). This suggests that the orientation of the two axial metal−ligand bonds in the two types of oxyCo subunits in the oxy Co−Fe hybrid Hbs is similar to those in oxyFe Hb.

Electron-Nuclear Coupling to Exchangeable ^2H. The issue of whether there is a hydrogen bond between the distal histidine and bound O_2 in both types of Hb subunits or only in the α subunits has been addressed by different techniques. An X-ray crystallographic study of oxyFe Hb (Shaanan, 1982, 1983) suggests that while a hydrogen bond between the distal histidyl N_ϵ-bound proton and the terminal oxygen atom of the heme-bound O_2 is possible in the α subunits, the distal histidine is too far from either oxygen atom of the bound O_2 for a hydrogen bond to form in the β subunits. This suggestion was considered to be consistent with the results of a RR study of oxyCo Hb, $(\alpha Co-O_2\beta Co-O_2)_2$ (Tsubaki & Yu, 1981), which assigned two different O−O bands on the basis of isotopic shifts. The frequency of one of these bands is close to the O−O band of model compounds, where there is no hydrogen bond to the bound O_2, while that of the other is lower. These results have been interpreted by Shannan (1983) as supporting the presence of a hydrogen bond to bound O_2 in oxyCo (and oxyFe) α subunits only. On the other hand, a RR study of the two oxy Fe−Co hybrid Hbs, $(\alpha Co-O_2\beta Fe-O_2)_2$ and $(\alpha Fe-O_2\beta Co-O_2)_2$ (Kitagawa et al., 1982), suggests that the distal hydrogen bond is present in both types of oxyCo subunits, on the basis of D_2O effects on ^{18}O-sensitive bands. (O−O bands of the oxyFe subunits are not observable by RR.) These contradictory findings are complicated by subsequent suggestions that the assignment of ^{18}O-sensitive bands in the RR spectra of oxyCo globins as pure O−O stretching modes is questionable because these bands are found to be coupled to other proximal histidyl imidazole and/or distal histidyl imidazole-related bands (Proniewicz & Kinkaid, 1990). Therefore, any D_2O effects cannot be used as an indication of modulation of the O−O bond alone (Bruha & Kincaid, 1988) nor as direct evidence for a hydrogen bond to bound O_2. On the other hand, one might infer the presence of a hydrogen bond to bound O_2 in the oxyCo subunits of the

oxy Co−Fe hybrid Hbs from the fact that the RR bands appear at lower frequencies than their counterparts in oxyCo porphyrin model compounds, where the hydrogen bond to the bound O_2 is absent (Bruha & Kincaid, 1988).

ESEEM studies of oxyCo globins in D_2O have been used to detect hydrogen bonds to bound O_2 (Lee et al., 1992, 1993, 1994a). As the unpaired electron of the paramagnetic center resides mainly on the bound O_2 (Hoffman et al., 1970; Getz et al., 1975; Dedieu et al., 1976; Tovrog et al., 1976), any observable ^2H electron-nuclear hyperfine (contact) interaction can be attributed to a bonding interaction between the bound O_2 and the coupled ^2H (Lee et al., 1992). The present ESEEM study of the two oxy Fe−Co hybrid Hbs in D_2O detects hyperfine-coupled ^2H in both types of oxyCo subunits[5] and supports the conclusion of Kitagawa et al. (1982) that a hydrogen bond to bound O_2 is present in both oxyCo α and oxyCo β subunits.

For oxyFe Hb, it has been suggested that since the distal histidyl N_ϵ is 2.7 Å from the terminal oxygen in the α subunits and at 3.2 and 3.4 Å from the directly coordinate oxygen and terminal oxygen atom, respectively, in the β subunits (Shanaan, 1982, 1983), a distal histidine−O_2 hydrogen bond is expected only in the α subunits. This suggestion is reasonable if oxyFe sw Mb is used as a model for the evaluation of distal hydrogen bonding. A neutron diffraction study of oxyFe sw Mb in D_2O (Phillips & Schoenborn, 1981) finds the distance between the terminal oxygen atom of heme-bound O_2 and the distal histidyl N_ϵ-bound deuterium to be 1.98 Å. This hydrogen bond in oxyFe sw Mb is considered to be of medium strength (Phillips & Schoenborn, 1981). A hydrogen bond of similar strength is expected in the α subunits of oxyFe Hb since its distal histidine−O_2 distance is similar to that in oxyFe sw Mb, 2.97 Å (Phillips, 1980). As the distance between bound O_2 and the N_ϵ of the distal imidazole is larger in the β subunits, the hydrogen bond is expected to be weaker. At present, there does not appear to be a likely explanation for the proposed subunit difference in the distal hydrogen bonding in oxyFe Hb that is not found for the oxy Fe−Co hybrid Hbs. On the other hand, the smaller Co−O−O bond angle in the oxyCo subunits of the hybrid Hbs, as compared to the Fe−O−O bond angle in their oxyFe counterparts in oxyFe Hb, would suggest that at least the terminal oxygen is further away from the distal histidine in the oxyCo subunits of the hybrid Hbs than in the oxyFe subunits of oxyFe Hb. This should make a hydrogen bond between the bound O_2 and the distal histidine more improbable in the oxyCo β subunits of $(\alpha Fe-O_2\beta Co-O_2)_2$ Hb, and yet spectroscopic evidence for one was found.

Summary. This ESEEM study reveals differences in electronic structure between the oxyCo subunits in $(\alpha Co-O_2\beta Fe-O_2)_2$ Hb and $\alpha(Fe-O_2\beta Co-O_2)_2$ Hb that suggest that (i) the Co−O_2 bond is more ionic in the oxyCo α subunits, which is consistent with the higher O_2 affinity[2] found for the Co α than for the Co β subunits, (ii) the Co−proximal histidyl N_ϵ and the Co−O_2 bonds are shorter in the oxyCo α subunits than in the oxyCo β subunits, and (iii) the Co−O−O bond angle is similar in the two types of oxyCo subunits and is smaller than that in oxyCo sw Mb. The X-ray crystal structure of oxyFe Hb (Shanaan, 1982, 1983) also shows shorter Fe−N_ϵ and Fe−O_2 bonds in the α subunits than in the β subunits while the Fe−O−O bond angle is similar in both types of subunits. Thus, besides matching a previously proposed relationship between electronic structure and O_2 affinity (Lee et al., 1992, 1993, 1994a), the oxyCo subunits in the two oxyCo−Fe hybrid Hbs also bear molecular features analogous to those of the subunits of oxyFe Hb shown in the X-ray crystal structure (Shaanan, 1982, 1983).

[5] In a preliminary report (Lee et al., 1994b), it was suggested that a hydrogen bond to bound O_2 in the oxyCo β subunits of $(\alpha Fe-O_2\beta Co-O_2)_2$ Hb is either absent or very weak due to the failure in detecting hyperfine-coupled ^2H in data collected between 8.5 and 9.9 GHz. The presence of hyperfine-coupled ^2H is confirmed in the present study by measurements at 10.7 GHz, using a microwave cavity of improved sensitivity.

REFERENCES

Ashby, C. I. H., Cheng, C. P., & Brown, T. L. (1978) *J. Am. Chem. Soc. 100*, 6057.

Belford, R. L., & Nilges, M. J. (1979) presented at the International Electron Paramagnetic Resonance Symposium, 21st Rocky Mountain Conference, Denver, CO.

Britt, R. D., & Klein, M. P. (1987) *J. Magn. Reson. 74*, 535.

Bruha, A., & Kincaid, J. R. (1988) *J. Am. Chem. Soc. 110*, 6006.

Cornelius, J. B., McCracken, J., Clarkson, R. B., Belford, R. L., & Peisach, J. (1990) *J. Phys. Chem. 94*, 6977.

Dedieu, A., Rohmer, M.-M., & Veillard, A. (1976) *J. Am. Chem. Soc. 98*, 5789.

Fermi, G. (1975) *J. Mol. Biol. 97*, 237.

Fermi, G., Perutz, M. F., Dickinson, L. C., & Chien, L. C. D. (1982) *J. Mol. Biol. 155*, 495.

Fermi, G., Perutz, M. F., Shaanan, B., & Fourme, R. (1984) *J. Mol. Biol. 175*, 159.

Flanagan, H. L., & Singel, D. J. (1987) *J. Chem. Phys. 87*, 5606.

Getz, D., Melamud, E., Silver, B. L., & Dori, Z. (1975) *J. Am. Chem. Soc. 97*, 3846.

Hoffman, B. M., & Petering, D. H. (1970) *Proc. Natl. Acad. Sci. U.S.A. 67*, 637.

Hoffman, B. M., Diemente, D. L., & Basolo, F. (1970) *J. Am. Chem. Soc. 92*, 61.

Hori, H., Ikeda-Saito, M., & Yonetani, T. (1980) *Nature 288*, 501.

Hori, H., Ikeda-Saito, M., & Yonetani, T. (1982) *J. Biol. Chem. 257*, 3636.

Hsieh, Y.-N., Rubenacker, G. V., Cheng, C. P., & Brown, T. L. (1977) *J. Am. Chem. Soc. 99*, 1384.

Ikeda-Saito, M., & Yonetani, T. (1980) *J. Mol. Biol. 138*, 845.

Ikeda-Saito, M., Yamamoto, H., & Yonetani, T. (1977) *J. Biol. Chem. 252*, 8639.

Imai, K., Ikeda-Saito, M., Yamamoto, H., & Yonetani, T. (1980) *J. Mol. Biol. 138*, 635.

Kitagawa, T., Ondrias, M. R., Rousseau, D. L., Ikeda-Saito, M., & Yonetani, T. (1982) *Nature 298*, 869.

Lee, H. C., Ikeda-Saito, M., Yonetani, T., Magliozzo, R. S., & Peisach, J. (1992) *Biochemistry 31*, 7274.

Lee, H. C., Wittenberg, J. B., & Peisach, J. (1993) *Biochemistry 32*, 11500.

Lee, H. C., Peisach, J., Dou, Y., & Ikeda-Saito, M. (1994a) *Biochemistry 33*, 7609.

Lee, H. C., Tsuneshige, A., Yonetani, T., & Peisach, J. (1994b) *Biophys. J. 66*, A268.

Magliozzo, R. S., McCracken, J., & Peisach, J. (1987) *Biochemistry 26*, 7923.

Maurice, A. M. (1981) Ph.D. Thesis, University of Illinois, Urbana, IL.

McCracken, J., Peisach, J., & Dooley, D. M. (1987) *J. Am. Chem. Soc. 109*, 4064.

Mims, W. B. (1974) *Rev. Sci. Instrum. 45*, 1583.

Mims, W. B. (1984) *J. Magn. Reson. 59*, 291.

Mims, W. B., & Peisach, J. (1978) *J. Chem. Phys. 69*, 4921.

Mims, W. B., & Peisach, J. (1989) *Advanced EPR Applications in Biology and Biochemistry* (Hoff, A. J., Ed.) p 1, Elsevier Press, Amsterdam, Holland.

Nilges, M. J. (1979) Ph.D. Thesis, University of Illinois, Urbana, IL.

Peisach, J., Mims, W. B., & Davis, J. L. (1979) *J. Biol. Chem. 254*, 12379.

Petsko, G. A., Rose, D., Tsernoglou, D., Ikeda-Saito, M., & Yonetani, T. (1978) in *Frontiers of Biological Energetics* (Dutton, P. L., Scarpa, A., & Leigh, J. S., Jr., Eds.) p 1011, Academic Press, New York.

Phillips, S. E. V. (1980) *J. Mol. Biol. 142*, 531.

Phillips, S. E. V., & Schoenborn, B. (1981) *Nature 292*, 81.

Proniewicz, L. M., & Kincaid, J. R. (1990) *J. Am. Chem. Soc. 112*, 675.

Shaanan, B. (1982) *Nature 296*, 683.

Shaanan, B. (1983) *J. Mol. Biol. 171*, 31.

Tovrog, B. S., Kitko, D. J., & Drago, R. S. (1976) *J. Am. Chem. Soc. 98*, 5144.

Tsubaki, M., & Yu, N.-T. (1981) *Proc. Natl. Acad. Sci. U.S.A. 78*, 3581.

Tsuneshige, A., & Yonetani, T. (1994) *Methods Enzymol. 231*, 215.

Wayland, B. B., & Abd-Elmageed, M. E. (1974) *J. Am. Chem. Soc. 96*, 4809.

Yonetani, T., Yamamoto, H., & Woodrow, G. V., III (1974a) *J. Biol. Chem. 249*, 682.

Yonetani, T., Yamamoto, H., & Iizuka, T. (1974b) *J. Biol. Chem. 249*, 2168.

BI942826H